Properties and sensing characteristics of surface-plasmon resonance in infrared light

Sergiy Patskovsky, Andrei V. Kabashin, and Michel Meunier

Laser Processing Laboratory, Department of Engineering Physics, Ecole Polytechnique de Montreal, Case Postale 6079, Succ. Centre-ville, Montreal, Quebec H3C 3A7, Canada

John H. T. Luong

Biotechnology Research Institute, National Research Council Canada, Montreal, Quebec H4P 2R2, Canada

Received December 3, 2002; revised manuscript received March 4, 2003; accepted March 20, 2003

Conditions of surface-plasmon resonance (SPR) production with use of IR pumping light (800–2300 nm) in the Kretschmann–Raether prism arrangement were investigated. Both calculations and experimental data showed that SPR characteristics in the IR are strongly influenced by the properties of the coupling prism material. Indeed, quite different regularities of plasmon excitation, polarity of sensing response, and sensitivity are observed for two different glasses and silicon. The observed differences in SPR properties are related to essentially different behavior of dispersion characteristics of materials near the SPR coupling point. Methods for improving sensor performance and miniaturizing the SPR technique using novel coupling materials (silicon) are discussed.

OCIS codes: 240.6680, 120.4820, 310.6860.

1. INTRODUCTION

Surface-plasmon resonance (SPR) is a prominent optical phenomenon that consists of a resonant transfer of the pumping light energy to a surface-plasmon mode coupled to collective oscillations of electrons in a metal.[1] The plasmons exist at a metal–dielectric interface and obey the following dispersion relation for two homogeneous semi-infinite media:

$$k_{\mathrm{SP}_0} = \frac{\omega}{c}\left[\frac{\epsilon_m(\omega)\epsilon_s(\omega)}{\epsilon_m(\omega) + \epsilon_s(\omega)}\right]^{1/2}, \tag{1}$$

where $k_{\mathrm{SP}_0} = k'_{\mathrm{SP}_0} + i\Gamma_i$ is a wave vector of surface plasmons (Γ_i is the intrinsic loss term), ϵ_m and ϵ_s are dielectric constants of the metal and dielectric medium, respectively, ω is the wave frequency, and c is the velocity of light. As shown schematically in Fig. 1(a), SPR is generally produced in the Kretschmann–Raether prism arrangement,[2,3] in which p-polarized visible light is directed through a glass prism and then reflected from a gold film deposited on the prism surface. The SPR effect causes an angular (spectral) dip of reflectivity that is due to the plasmon excitation, and this dip position is extremely sensitive to the dielectric constant ϵ_s of the adjacent medium in a thin layer near the interface. The high sensitivity exhibited by the SPR effect is now widely employed in biological and chemical sensing.[4–6] With a biomolecule or receptor covalently immobilized on the metal surface, a change of SPR parameters can reflect variations of the sensing layer thickness that are due to a selective interaction between the biomolecule and its analyte partner from an aqueous solution.[7] Recording angular,[4–6] wavelength,[8,9] or phase[10–12] characteristics of the reflected light, SPR biosensors offer the opportunity for real-time and label-free monitoring of biomolecular interactions. Most known SPR-based systems operate with visible light and have a probe depth of ~200–300 nm, i.e., the layer thickness within the sensible response. Reviews of studies of biological interactions using SPR techniques are available in the literature.[7,13,14]

It has been known that increasing the wavelength of the pumping light leads to a decrease of dissipation in the system and the generation of long-propagation plasmons.[1,15] These plasmons have remarkably different parameters of excitation in the near-IR range (700–1200 nm) and offer certain advantages for sensing (see, e.g., Refs. 16–20). First, the probe depth of these plasmons can reach 1.5–2 μm,[18] which in turn improves the resulting sensitivity of the system for recording biological or chemical interactions. Then, long-propagation plasmons are generated under a narrower range of angles (wavelengths), which contributes to better accuracy of SPR dip-position measurements.[19,20] Furthermore, SPR excitation with IR light in a wider range (>1100 nm) might provide some extra opportunities, such as the use of novel advanced materials for coupling and improved sensor characteristics. As silicon is transparent in this range, its use is very appealing with respect to sensor miniaturization and integration. However, the development of silicon-based SPR sensors requires the determination of conditions of SPR excitation in the IR range as a prerequisite, since dispersion effects become important in this range. This paper is devoted to the consideration of basic conditions of SPR excitation in the IR range (800–2300 nm) using the Kretschmann–Raether geometry. Two different glasses (BK7 and SF11) and silicon are examined as prism materials.

1084-7529/2003/081644-07$15.00

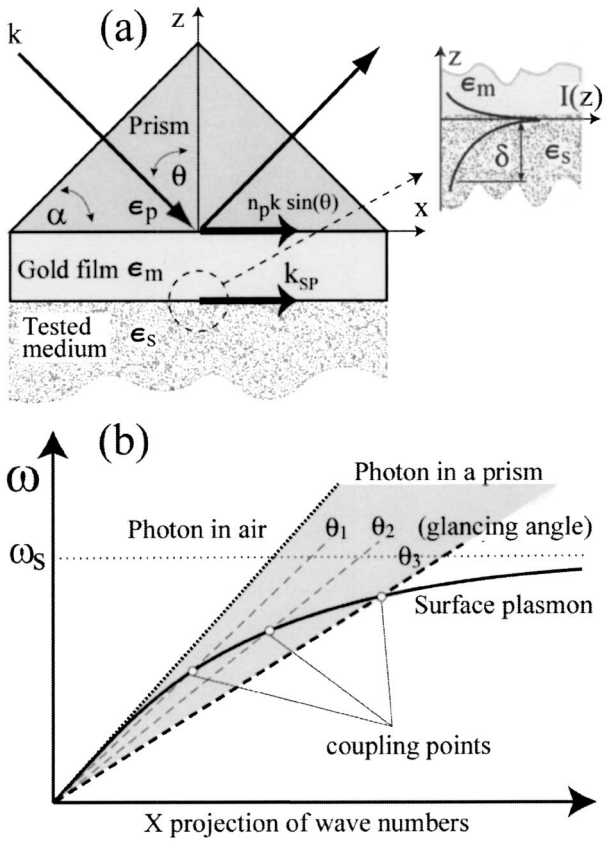

Fig. 1. (a) Schematic of the three-layer system (prism–gold film–sensing medium) used in the calculations and experiment. (b) Dispersion curves $\omega(k_x)$ of surface plasmons over a metal–dielectric (tested medium) interface and that of the photons in coupling (prism) materials.

2. THEORETICAL FRAMEWORK

In the Kretschmann–Raether prism arrangement,[2,3] light is directed to a gold film through a glass prism with a relatively high refractive index n_p, as shown in Fig. 1(a). The prism is usually coated with a gold film such that the prism–metal and metal–dielectric interfaces are the optimum distance apart. The energy can be transferred by matching the projection of the wave number of the incident beam on the surface k_x to the surface-plasmon wave number k_{SP} at a specific combination of the pumping frequency ω and the angle of incidence θ_{SPR}:

$$n_p \frac{\omega}{c} \sin \theta_{\mathrm{SPR}} = k_{\mathrm{SP}}. \tag{2}$$

The physical meaning of the phenomenon becomes clearer if we consider the wave number projections for all involved waves on the interface (x axis). From the dependence $\omega(k_x)$ depicted in Fig. 1(b), the surface-plasmon mode can be excited at all frequencies below the surface-plasmon frequency ω_s, which is in the green range for gold.[15] For photons in a dielectric prism, the dispersion relations $\omega = ck/n_p$ represent lines whose slope with respect to the abscissa increases with an increase in the refractive index n_p. It is evident that the maximal x-axis projection of the lines is achieved under glancing angles of incidence of about 90° [Fig. 1(a)]. In the diagram of $\omega(k_x)$, coupling takes place at the intersection between the plasmon curve and the photon curve [Fig. 1(b)]. For photons in air, the slope is not sufficient to match the wave numbers of the plasmon to the photon. However, the matching and energy transfer to the plasmon mode might still be feasible if a prism with a higher refractive index were used.

The wave number k_{SP} is generally different from the wave number of ideal surface plasmons determined by Eq. (1), since the system is perturbed by the presence of the prism and the finiteness of the layers. A precise solution for parameters of light reflected from an arbitrary multilayer system can be obtained from Fresnel equations, which give the result in the form of an electromagnetic field distribution. However, the calculation of the dispersion relation by Fresnel equations is rather time-consuming since every point on the dispersion curve must be determined individually. In this study, we consider the phenomenon in the framework of a model of plasmon oscillations. The system perturbation due to the presence of the prism and the finiteness of layers is taken into consideration by the introduction of the loss-term wave number $k_r = k_r' + i\Gamma_r$ (Γ_r is a reradiative loss term), and the complex wave vector of the surface plasmons can be expressed as[2,21,22]

$$k_{\mathrm{SP}} = k_{\mathrm{SP}_0} + k_r, \tag{3}$$

where k_{SP_0} is the wave number in the absence of the prism as determined by Eq. (1). The expression for the loss-term wave number k_r in the prism configuration has been derived through the parameters of layers[21]:

$$k_r = -\frac{\omega}{c}[r_{\mathrm{pm}}(k_x = k_{\mathrm{SP}_0})]\left(\frac{2}{\epsilon_m - \epsilon_s}\right) \times \left(\frac{\epsilon_m \epsilon_s}{\epsilon_m - \epsilon_s}\right)^{3/2} \exp\left[i\frac{4\pi d}{\lambda}\frac{\epsilon_m}{(\epsilon_m + \epsilon_s)^{1/2}}\right], \tag{4}$$

where r_{pm} is the reflectance of the p-polarized component obtained from Fresnel equations, d is the gold layer thickness, and λ is the pumping wavelength. A solution of Eq. (2) through the pumping wavelength λ and θ_{SPR} permits the determination of the SPR conditions. The plasmon model also permits the characterization of SPR reflectivity curves. The reflectivity in the immediate vicinity of the resonance R, and the width of the SPR dip W_k, can be expressed, respectively, as[2]

$$R = 1 - \frac{4\Gamma_i \Gamma_r}{(k_x - k_{\mathrm{SP}}')^2 + (\Gamma_i + \Gamma_r)^2}; \qquad W_K = \frac{2(\Gamma_i + \Gamma_r)}{n_p \frac{\omega}{c} \cos \theta_{\mathrm{SPR}}}. \tag{5}$$

However, consideration of the system in the IR range requires a detailed account of the dispersion characteristics of all materials, including those of the prism. In contrast to the case for visible light, these properties can play a crucial role in the formation of SPR characteristics. In this study, we consider two typical examples of testing medium: air and water. The dispersion relation for wa-

ter was obtained from an equation given by Harvey *et al.*,[23] whereas a correction factor for weak water absorption was obtained from the data of Kou *et al.*[24] Dispersion properties of gold in visible and IR light were taken from the data of Innes and Sambles[25] and Johansen *et al.*[18] We considered three different prism materials: BK7 and SF11 glasses and silicon. The dispersion characteristics for BK7 and SF11 glasses were taken from the data of the supplier (Melles Griot, Irvine, Calif.). The optical constants for silicon were obtained from the approximation of experimental dependencies reported by Herzinger and co-workers.[26]

Finally, the reflectivity in the SPR resonance dip can be minimized in the Kretschmann–Raether prism configuration by optimizing the thickness of the gold film[21]:

$$d_{\mathrm{opt}} = \frac{\lambda}{4\pi} \frac{1}{\sqrt{|\epsilon_m'|}\left(1 + \frac{\epsilon_s}{2|\epsilon_m'|}\right)} \ln\left(\frac{4|\epsilon_m'|\sin\varphi}{\epsilon_m''}\right),$$

$$\tan\frac{\phi}{2} \cong \frac{\epsilon_p}{\sqrt{(|\epsilon_m'|(\epsilon_p - \epsilon_s) - \epsilon_p\epsilon_s)}}. \quad (6)$$

3. EXPERIMENTAL SETUP

To verify the validity of the performed calculations, we carried out a series of experiments in the Kretschmann–Raether prism arrangement [Fig. 1(a)]. The SPR coupling system consisted of a prism, a gold film, and a flow cell (empty or filled with distilled water, depending on the aqueous or gaseous tested medium). In the experiments, BK7 and SF11 glass prisms were used with the base angle of $\alpha = 45°$ for gaseous and $\alpha = 60°$ for aqueous tested media [Fig. 1(a)]. In addition, the silicon prisms (p-type, $R > 20\ \Omega$ cm, Almaz Optics, West Berlin, N.J.) with $\alpha = 16.6°$ and $\alpha = 22.4°$ were specially designed for experiments with the gaseous and aqueous tested medium, respectively. With such prisms, it was feasible to attain the incidence of the laser beam on the silicon–gold interface at angles close to θ_{SPR} from the calculation. Gold films were deposited on the prisms. In addition, for some test experiments the gold was deposited on a 1-mm-thick glass slide or 0.5-mm-thick silicon wafer, which was then placed in immersion contact with the prism. Light pressure was applied to the immersion liquid to provide better optical contact. The thickness of gold film was optimized by use of Eq. (6). The value of 40 nm was selected to ensure minimal reflectivity in resonant conditions in the range 1100–1700 nm for all three prisms. The SPR coupling system (with or without the flow cell) was placed onto a rotary block of a variable-angle spectroscopic ellipsometer (Woollam VASE® ellipsometer, J. A. Woollam, Lincoln, Neb.) to allow for very fine variation of the angular prism position with respect to the optical path of the ellipsometer. The system was illuminated by continuous monochromatic p-polarized light with variable wavelength, obtained by passing white light from a 75-W xenon lamp source through a monochromator with an extended spectral range (240–1700 nm). The light reflected from the coupling system was analyzed by a detector whose characteristics were normalized to take into account the spectral response of the light source. The experiments were performed with a configuration of either wavelength or incident angle fixed. The precision of angular and spectral measurements was 0.005° and 0.1 nm, respectively. All experiments were performed at room temperature.

4. RESULTS AND DISCUSSION

The calculations and experimental data revealed that the SPR effect could be produced for all prism materials including silicon, albeit with the silicon prism, the surface plasmons were excited only at wavelengths above 1100 nm. Figure 2 presents typical angular reflectivity curves from the theory (dashed curves) and experimental data (solid curves) for three different prism materials, which were used for sensing in the (a) gaseous and (b) aqueous medium. As shown by the experimental curves, the angles were related to the prism–gold interface, while a slight light refraction at the entrance to the prism was taken into account as a correction coefficient. It was obvious that the main trend of theoretical prediction was well confirmed by relevant experimental data. Indeed, the calculated and measured positions of reflectivity minimum were almost identical for all prism materials, which confirms the validity of the applied plasmon model used in our calculations and the relative precision of the dispersion data obtained from previous studies.

As shown in Figs. 2(a) and 2(b), the SPR effect was achieved at quite different angles of incidence θ for differ-

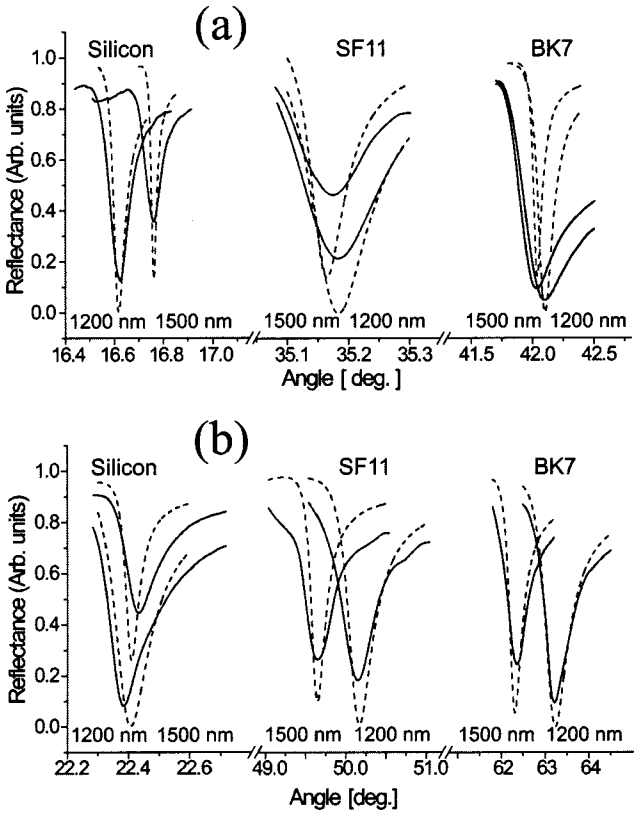

Fig. 2. Typical angular reflectivity curves for prisms from BK7 and SF11 glasses and silicon in the configuration of (a) gaseous and (b) aqueous sensing medium. The dashed and solid curves correspond to the calculated and experimental data, respectively.

ent prism materials, depending upon their refractive index n_p. In this case, n_p increased with a decrease in the resonant angle θ_{SPR}. For example, in the gaseous medium the values of θ_{SPR} were ~42°–46° for BK7 glass ($1.5 < n_p < 1.55$), 35°–38° for SF11 glass ($1.7 < n_p < 1.8$), and 16.5°–16.8° for silicon ($3.45 < n_p < 3.7$), while those of the aqueous medium were 60°–80°, 50°–55°, and 22°–25°, respectively. The width of the reflectivity minima decreased with an increase of the prism refractive index; the result was especially remarkable for the calculated curves. For example, in the gaseous sensing medium, the calculated FWHM at $\lambda = 1200$ nm was about 0.156° (versus 0.3° for the experiment) for BK7 glass, 0.126° (0.2° experiment) for SF11 glass, and 0.066° (0.12° experiment) for silicon, while for the aqueous medium the relevant values were 0.75° (0.8° experiment), 0.417° (0.5° experiment), and 0.16° (0.18° experiment), respectively. The recorded smaller width of the reflectivity curve for silicon was apparently attributable to its relatively high refractive index. Indeed, as indicated in Eq. (5), the higher the index of refraction n_p, the narrower the reflectivity curve. It is noteworthy that the experimental reflectivity curves were somewhat broader compared with the theoretical ones. For aqueous medium, the difference of curve widths was relatively small, whereas for gaseous medium the experimental curves were broader by a factor of ~2 for all prisms. The broadening was probably related to properties of the gold films used, and could be explained by a surface roughness or nonuniformity of the film thickness in the light spot. Indeed, roughness can lead to a certain increase in the imaginary part of the plasmon wave number Γ_i, whereas the nonuniformity can increase the loss term wave number Γ_r. Both mechanisms increase the numerator of Eq. (5) and, consequently, the curve width W_k for all three prism materials by the same factor. Since the resonant curve is originally broadened for the aqueous sensing medium in comparison with the gaseous one, the effect of broadening is less pronounced for this medium. A certain error in the data on gold's refractive index used in our calculations and a divergence of light source beam in the experiments could partly contribute to the discrepancy between experimental and theoretical curve widths.

The position of the reflectivity minimum for each prism material was strongly dependent on the wavelength λ of pumping light, as shown in Figs. 2(a) and 2(b). For each wavelength, an appropriate angle of incidence θ could be chosen to provide resonant conditions. However, the angular shift due to the increase of λ was opposite for silicon and the glasses. Similar minimum values could be observed in the spectral dependence of the reflectivity when the angle of incidence was fixed. In this case, the position of the spectral minimum was very sensitive to the angle of incidence. For example, with the silicon prism, a slight decrease of the incident angle from 16.9° to 16.5° led to a considerable shift of the reflectivity minimum to shorter wavelengths. The data for the SPR minimum position collected from the angular and spectral reflectivity curves are summarized in Figs. 3(a) and 3(b), which describe the resonant conditions for a simultaneous variation in λ and θ. The theoretical SPR minimum angle and wavelength could be generated from these plots by taking

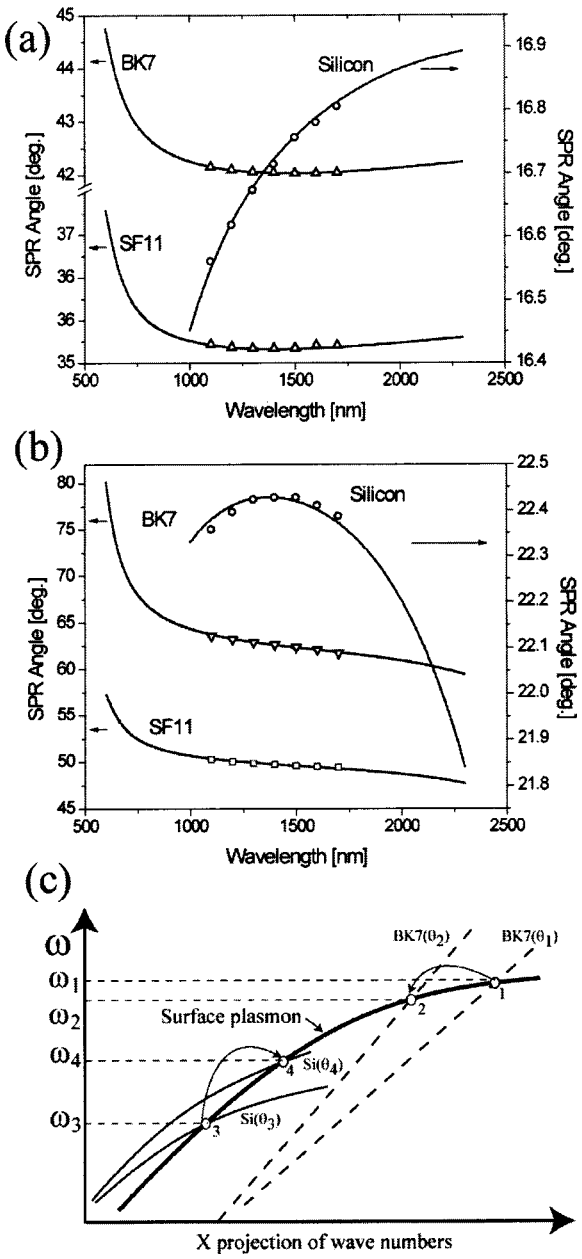

Fig. 3. SPR dispersion curves for different prism materials (BK7 and SF11 glasses and silicon) in the configuration of (a) gaseous and (b) aqueous sensing medium. The contours show conditions of minimal reflectivity as a function of wavelength λ and angle of incidence θ. The symbols represent the experimental data, while the curves depict the results of calculations. (c) Descriptive behavior of dispersion curves $\omega(k_x)$ of surface plasmons and photons in BK7 glass (BK7) and silicon (Si) prisms near the coupling points (1–4).

a cut parallel to the y or x axis. As illustrated in this figure, the SPR dispersion curves revealed a striking difference between glass and silicon. For BK7 or SF11 glass, θ decreased with an increase in the wavelength λ for the pumping light up to 800 nm. Beyond this wavelength, the angle of incidence became less sensitive to any further change in λ. In the gaseous medium, the indicated tendency changed to the opposite direction when $\lambda > 1200$ nm was used for pumping. In particular, for BK7 this phenomenon led to the appearance of two peaks

at ~1200 nm and 1900 nm in the spectral reflectivity curves recorded at a fixed angle of ~42.1°.

However, the use of silicon as the sensing prism resulted in quite different behavior of SPR excitation. In air, the increase in wavelength was accompanied by an increase in the resonant angle [Fig. 3(a)] that was completely opposite to the case of glasses. In aqueous medium, such behavior was even more surprising, as illustrated in Fig. 3(b). The resonant angle initially increased with an increase in the wavelength and reached a maximum value at $\lambda = 1400$ nm. The angle of resonance then decreased with a further increase in λ. Such behavior indicated that with a resonant angle below 22.4°, there were two dips in the IR range and the absolute angle variations were more pronounced in the visible range in comparison with IR. For glass, these variations in the range of 800–2200 nm did not exceed 1° and 5° for air and water, respectively, whereas the corresponding values for the visible range reached 3.5° and 12°–14°, respectively. The angular variation values in the IR range for silicon were even smaller, within only 0.8° regardless of a wide variation in λ (1000–2200 nm).

The above-mentioned striking difference in the dependencies for glasses and silicon could be explained by considering conditions of the wave number matching in terms of the dispersion $\omega(k_x)$ as depicted in Fig. 1(a). Qualitative behavior of the dispersion relations $\omega(k_x)$ for plasmons and photons in the prism in the vicinity of the coupling point is shown in Fig. 3(c). An attempt to obtain a precise solution of dispersion equations resulted in less illustrative plots because the convergence angles of curves near the coupling point were too small. For BK7 glass, the dependence $\omega(k_x)$ was linear (curves labeled BK7), while for silicon the dispersion relation exhibited a nonlinear relationship (solid curve). In both cases, the plots $\omega(k_x)$ approached the k_x axis with an increase in the angle of incidence (the closest position achieved at $\theta = 90°$). Considering the two curves BK7(θ_1) and BK7(θ_2), corresponding to two different angles of incidence with $\theta_1 > \theta_2$, the coupling could take place at these two points. The coupling points 1 and 2 corresponded to the pumping frequencies ω_1 and ω_2 with $\omega_1 > \omega_2$. Therefore, for BK7 glass, the incident resonant angle decreased with a decrease in ω or an increase in λ, consistent with the SPR dispersion curves presented in Fig. 3(a). For silicon, an opposite trend was anticipated by considering the two curves Si(θ_3) and Si(θ_4) at two different angles of incidence θ_3 and θ_4 with $\theta_3 > \theta_4$. As the coupling took place with $\omega_3 < \omega_4$, the pumping wavelength would decrease as θ decreased in accordance with the SPR dispersion curves [Fig. 3(a)]. Similarly, this argument could be used to explain the behavior of SPR dispersion curves obtained for sensing in the aqueous medium [Fig. 3(b)].

Hence the SPR effect could be reproduced in the IR range for different prism materials, while the prism-related dispersion phenomena determined the characteristics of all spectral and angular SPR dependencies. We observed that the insertion of any transparent parallel layer between a silicon prism and the gold film did not change the dependencies, provided the thickness of the layers was sufficiently large to nullify film interference effects. This phenomenon was apparently explained by the fact that the addition of an intermediate parallel layer did not change the tangential component of the wave number of the pumping wave [Fig. 1(a)] and therefore did not influence the conditions of SPR excitation. In other words, a silicon prism with a gold film on a glass slide (in immersion contact with the prism) should exhibit the same characteristics as the purely silicon-based scheme, i.e., the dispersion properties of silicon still govern all SPR characteristics. In contrast, a glass prism with a gold film on a silicon wafer displays the glass-related SPR characteristics, whereas silicon simply serves as a transparent material. This means a system with a silicon prism can be used with replaceable and cheap glass or silicon slides to simplify the design for practical sensing applications.

We compared sensitivities of infrared SPR schemes for three prism materials. In chemical and biological sensing schemes, the bulk refractive index of the adjacent gaseous ($n_s \sim 1$) or aqueous ($n_s \sim 1.33$) medium was considered constant during the measurement, while a thin chemical or biological film on the gold changed the resulting thickness because of a selective binding or recognition interaction. In the calculations, we considered the increase of the layer thickness d with a refractive index of $n_{\text{film}} = 1.1$ and $n_{\text{film}} = 1.42$ for the gaseous and aqueous sensing environment, respectively, consistent with the parameters used in chemical and biological sensing.[7] A change of resonant conditions due to changes of the thickness was recorded under the fixed pumping wavelength λ (angular interrogation) and the fixed incident angle θ (spectral interrogation). In this study, we examined sensing responses for the two interrogations separately.

In the scheme with a fixed λ, the "absolute" sensitivity represented a simple angular shift of the SPR dip due to a change in the thickness d. Figure 4 shows the change of the resonant angle θ_{SPR} as a function of d in a model of the (a) gas and (b) aqueous medium. For all three prisms, the angle θ_{SPR} was proportional to the film thickness. The response sensitivity to the thickness growth was also more pronounced for glass than silicon [Figs. 4(a) and 4(b)]. At a fixed angle θ, the result became more intriguing since the response of the silicon-based system was quite different from the trend observed for glass, as illustrated in Figs. 4(c) and 4(d). For glasses, the main trend was the increase of the resonant wavelength λ_{SPR} as the layer thickness d increased, which was valid for both the gas [Fig. 4(c)] and the aqueous [Fig. 4(d)] medium. However, silicon demonstrated an opposite tendency in the case of the gas medium, i.e., λ_{SPR} decreased with an increase in d [Fig. 4(c)]. In the aqueous medium, the system's response obtained for silicon was even more complicated and intriguing since the silicon prism resulted in two spectral dips if the angle of incidence was fixed at 22.3°–22.4° [Fig. 3(b)]. The dip at the relatively short wavelength $\lambda_{\text{SPR}} < 1400$ nm exhibited a decrease with an increase in d, while the long wavelength dip $\lambda_{\text{SPR}} > 1400$ nm showed an opposite trend. Consequently, the distance between the two dips became wider as the thickness of the sensing layers increased. Nevertheless, the spectral sensitivities were comparable for silicon and glasses in the case of the gaseous medium,

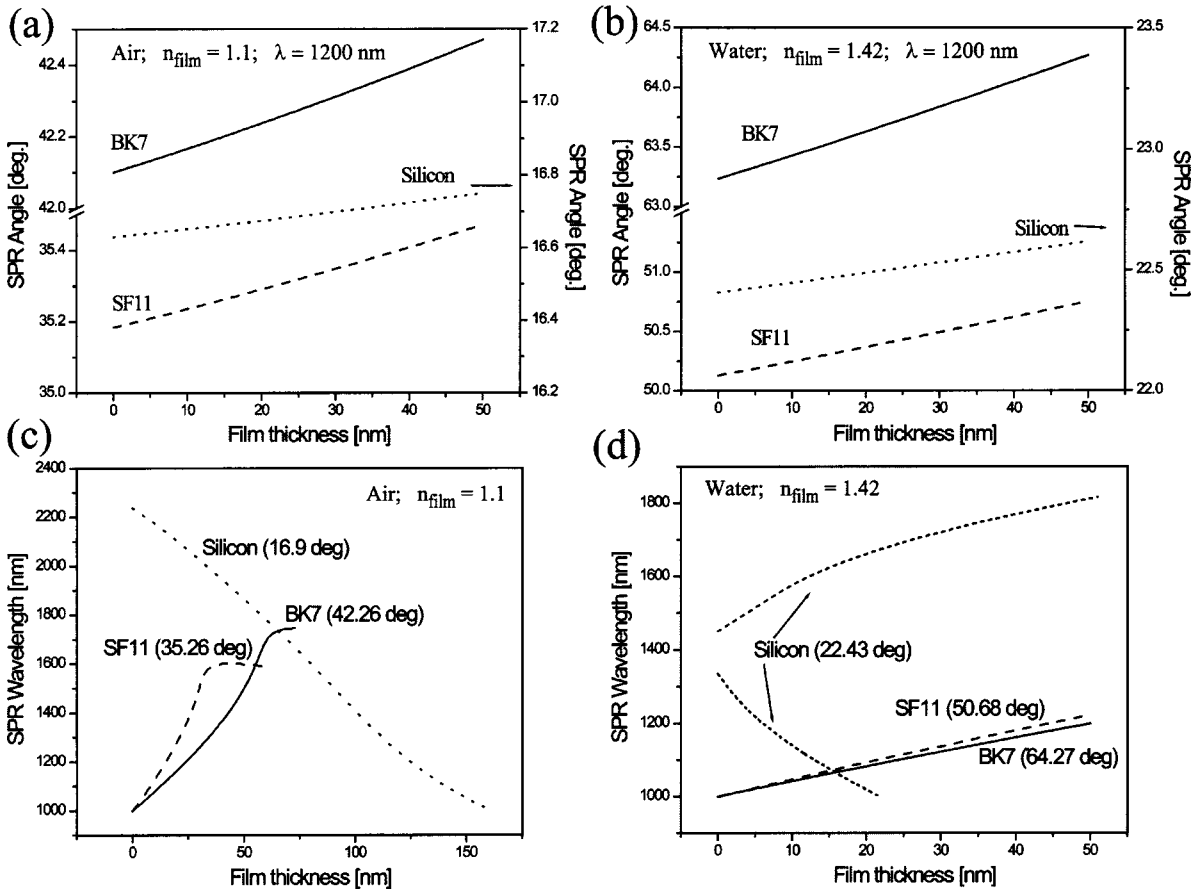

Fig. 4. Angular interrogation: angular sensing response of the system to the increase in film thickness of a dielectric layer with the refractive index $n_{film} = 1.1$ in the case of the sensing (a) in air and $n_{film} = 1.42$ in the case of the sensing (b) in water. The dependencies were obtained for the fixed pumping wavelength $\lambda = 1200$ nm. Spectral interrogation: spectral sensing response of the system to the increase in film thickness for (c) the gaseous and (d) aqueous sensing medium. The dependencies were obtained for the fixed angles of incidence.

whereas in the aqueous medium, silicon actually provided higher sensitivity.

The absolute sensitivity was not anticipated to provide a complete description of the sensing response since the position of relatively narrow reflectivity curves could be measured with higher precision using a high-resolution detection system.[19,20] In practice, high-precision measurements would improve the detection sensitivity.[18] In fact, we encountered such a situation in the case of the angular interrogation as the resonant curves became relatively narrow in the IR range (<0.1°), but they were still measurable with higher precision. For a complete description of such systems, many investigators use so-called intrinsic sensitivity, corresponding to the shift (angular or spectral) of the SPR dip divided by its width for a given change of the refractive index of the sensing medium.[18] Our calculation shows that for gold with a thickness close to d_{opt}, the intrinsic sensitivity became similar for both the glass and silicon prisms because the angular curves were narrower for silicon. Considering the resolution of modern goniometer systems is less than 0.0002°, the realization of this sensitivity is quite realistic and feasible. Thus schemes with glasses and silicon are expected to display the same polarity of sensing response for the angular sensitivity and the opposite polarity for the spectral sensitivity.

The polarity of the sensing response was also explained by the diagram with the dispersion relation $\omega(k_x)$ near the coupling point as presented in Fig. 3(c). The increase of the integral refractive index n_s due to the thickness increase led to a shift of the plasmon dispersion curve towards the k_x axis. Therefore it was necessary to increase the angle θ to restore the coupling conditions at a fixed frequency (angular sensitivity). For either glass or silicon, increasing d led to an increase in θ_{SPR}, in agreement with the dependencies of Figs. 4(a) and 4(b). For a fixed angle θ (spectral sensitivity), we anticipated the opposite response of two platforms as described in Fig. 4(c). To compensate for the shift of the surface plasmon curve with the increase in d, it is necessary to decrease the pumping frequency ω for the BK7 glass, but this operating parameter must be increased with silicon as the sensing prism.

As described previously, SPR in the IR was characterized by a much larger probe depth. This probe depth was almost insensitive to the properties of the prism material and reached 1.5–2 μm, while for the visible light the depth was limited to only 200–300 nm.[18] Therefore SPR schemes with IR light should be more efficient in remote sensing. From our perspective, this phenomenon might be used to record the sensing event far from the gold surface or to detect the interaction on the surface of large ob-

jects of relatively low refractive indices. Deadly viruses and bacteria are two important examples of such objects that cannot be detected by current visible-based SPR schemes. The concept of sensing on a silicon platform is especially attractive with respect to the ease of miniaturization of SPR systems, a key requirement for remote monitoring applications. Of course, the expectation is based on the fact that methods for microfabrication and circuit integration are well developed for silicon. Undoubtedly, the integration of the SPR-based transducer on a silicon-based processing chip will contribute to the development of novel, compact biosensors and microarrays.

5. CONCLUSIONS

On the basis of plasmon model and experimental data, we investigated the behavior of surface-plasmon resonance (SPR) in IR pumping light (800–2300 nm). SPR was produced in the Kretschmann–Raether prism arrangement with use of three different coupling materials: BK7 and SF11 glasses and silicon. It was demonstrated that the qualitative behavior of most SPR dependencies in the IR was strongly influenced by the dispersion properties of the involved materials. Compared with glass, the use of silicon as the sensing prism resulted in remarkably different SPR dispersion curves, opposite polarity of the SPR response, and increased sensitivity. Based on the sensing responses of angular and spectral schemes obtained with different coupling materials, SPR with IR light could be a distinct candidate for the improvement of SPR sensor performance in comparison with current SPR technology based on visible light.

ACKNOWLEDGMENTS

The authors thank Ludvik Martinu of the Department of Engineering Physics, Ecole Polytechnique de Montreal, for assistance with experimental facilities. We also acknowledge the financial contribution from the Natural Science and Engineering Research Council of Canada.

Corresponding author S. Patskovsky may be reached by e-mail at psv@canada.com.

REFERENCES

1. H. Raether, “Advances in Research and Development,” in *Physics of Thin Films*, G. Hass, M. H. Francombe, and R. W. Hoffmann, eds. (Academic, New York, 1997), pp. 145–261.
2. E. Kretschmann, “Decay of nonradiative surface plasmons into light on rough silver films. Comparison of experimental and theoretical results,” Opt. Commun. **6**, 185–187 (1972).
3. E. Kretschmann and H. Raether, “Radiative decay of nonradiative surface plasmons excited by light,” Z. Naturforsch. A **23**, 2135–2136 (1968).
4. B. Liedberg, C. Nylander, and I. Lundstrum, “Surface-plasmon resonance for gas detection and biosensing,” Sens. Actuators B **4**, 299–304 (1983).
5. B. Liedberg, C. Nylander, and I. Lundstrom, “Biosensing with surface-plasmon resonance–how it all started,” Biosens. Bioelectron. **10**, i–ix (1995).
6. J. L. Melendez, R. Carr, D. U. Bartholomew, K. A. Kukanskis, J. Elkind, S. S. Yee, C. E. Furlong, and R. G. Woodbury, “A commercial solution for surface-plasmon sensing,” Sens. Actuators B **35**, 212–216 (1996).
7. P. Schuck, “Use of surface-plasmon resonance to probe the equilibrium and dynamic aspects of interactions between biological macromolecules,” Annu. Rev. Biophys. Biomol. Struct. **26**, 541–566 (1997).
8. L. M. Zhang and D. Uttamchandani, “Optical chemical sensing employing surface-plasmon resonance,” Electron. Lett. **23**, 1469–1470 (1988).
9. R. C. Jorgenson and S. S. Yee, “Fiber-optic chemical sensor based on surface plasmon resonance,” Sens. Actuators B **12**, 213–220 (1993).
10. F. Abeles, T. Lopez-Rios, and A. Tadjeddine, “Investigation of the metal-electrolyte interface using surface-plasma waves with ellipsometric detection,” Solid State Commun. **16**, 843–847 (1975).
11. A. V. Kabashin and P. I. Nikitin, “Surface-plasmon resonance interferometer for bio- and chemical-sensors,” Opt. Commun. **150**, 5–8 (1998).
12. A. N. Grigorenko, P. I. Nikitin, and A. V. Kabashin, “Phase jumps and interferometric surface-plasmon resonance imaging,” Appl. Phys. Lett. **75**, 3917–3919 (1999).
13. P. B. Garland, “Optical evanescent wave methods for the study of biomolecular interactions,” Q. Rev. Biophys. **29**, 91–117 (1996).
14. S. Lofas, “Dextran modified self-assembled monolayer surfaces for use in biointeraction analysis with surface-plasmon resonance,” Pure Appl. Chem. **67**, 829–834 (1995).
15. V. M. Agranovich, D. L. Mills, eds., *Surface Polaritons Electromagnetic Waves at Surfaces and Interfaces* (North-Holland, Amsterdam, 1982).
16. H. de Bruijn, R. Kooyman, and J. Greve, “Choice of metal and wavelength for surface-plasmon resonance sensors: some considerations,” Appl. Opt. **31**, 440–442 (1992).
17. R. C. Jorgenson, C. Jung, S. S. Yee, and L. W. Burgess, “Multi-wavelength surface-plasmon resonance as an optical sensor for characterizing the complex refractive indices of chemical samples,” Sens. Actuators B **14**, 721–722 (1993).
18. K. Johansen, H. Arwin, I. Lundström, and B. Liedberg, “Imaging surface-plasmon resonance sensor based on multiple wavelengths: sensitivity considerations,” Rev. Sci. Instrum. **71**, 3530–3538 (2000).
19. A. G. Frutos, S. C. Weibel, and R. M. Corn, “Near-infrared surface-plasmon resonance measurements of ultrathin films. 2. Fourier transform SPR spectroscopy,” Anal. Chem. **71**, 3935–3940 (1999).
20. B. P. Nelson, A. G. Frutos, J. M. Brockman, and R. M. Corn, “Near-infrared surface-plasmon resonance measurements of ultrathin films. 1. Angle shift and SPR imaging experiments,” Anal. Chem. **71**, 3928–3934 (1999).
21. K. Kurihara and K. Suzuki, “Theoretical understanding of an absorption-based surface-plasmon resonance sensor based on Kretschmann’s theory,” Anal. Chem. **74**, 696–671 (2002).
22. E. M. Yeatman, “Resolution and sensitivity in surface-plasmon microscopy and sensing,” Biosens. Bioelectron. **11**, 635–649 (1996).
23. A. H. Harvey, J. S. Gallagher, and J. M. H. Levelt-Sengers, “Revised formulation for the refractive index of water and steam as a function of wavelength, temperature and density,” J. Phys. Chem. Ref. Data **27**, 761–774 (1998).
24. L. Kou, D. Labrie, and P. Chylek, “Refractive indices of water and ice in the 0.65–2.5-mm spectral range,” Appl. Opt. **32**, 3531–3540 (1993).
25. R. A. Innes and J. R. Sambles, “Optical characterization of gold using surface-plasmon polaritons,” J. Phys. F **17**, 277–287 (1987).
26. C. M. Herzinger, B. Johs, W. A. McGahan, J. A. Woollam, and W. Paulson, “Ellipsometric determination of optical constants for silicon and thermally grown silicon dioxide via a multi-sample, multi-wavelength, multi-angle investigation,” J. Appl. Phys. **83**, 3323–3336 (1998).